Pulicaria odora Ethanolic Extract as a Corrosion Inhibitor and Its Eco-friendly Synthesis of CuO Nanoparticles for Photocatalytic and Microbial Properties



K. Dob, a,b,* D. Zouied, c,d M. Khelfaoui, d,d N. Bouzenad, d,e A. Abdennouri, d,e and M. Rouainia c,f

^aDepartment of Technology, Faculty of Technology,

20 August 1955 University Skikda, Algeria

^bLaboratory of Stimulation and Biological and Environmental Processes,

University-20 August-1955-Skikda, Algeria

^cLaboratory LGCES, Faculty of Technology, 20 August 1955 University,

El-Hadaeik Road, P.O. Box 26, Skikda 21000, Algeria

^dDepartment of Process Engineering, Faculty of Technology, 20 August 1955

University, P.O. Box 26, Skikda 21000, Algeria

^eLaboratory of Catalysis, Bioprocess and Environment,

Department of Process Engineering, Faculty of Technology,

University of 20 August 1955, Skikda 21000, Algeria

^fDepartment of Petrochemistry, Faculty of Technology, 20 August 1955

University of Algiers, B.P. 26, Skikda 21000, Algeria

doi: https://doi.org/10.15255/CABEQ.2025.2429

Original scientific paper Received: May 17, 2025 Accepted: September 8, 2025

This work examines the effect of *Pulicaria odora* leaf extract effect as a green inhibitor on SS308 steel corrosion in a 1 mol L⁻¹ hydrochloric acid solution. The electrochemical results reveal that inhibitory efficiency increases with the concentration of *Pulicaria odora* leaf extract, reaching a maximum inhibition rate of 94.6 % at 500 ppm. Potentiodynamic polarization curves suggest that the plant extract acts as an anodic-type inhibitor. The polarization and electrochemical impedance findings are in good agreement. Adsorption of the inhibitor on the steel surface is spontaneous and follows the Langmuir isotherm. Furthermore, a copper-based catalyst synthesized using *Pulicaria odora* extract produced a good yield, and this catalyst showed effective photodegradation of methylene blue. The CuO nanoparticles (NPs) synthesized from *Pulicaria odora* extract showed significant antimicrobial activity against the tested bacterial strains.

Keywords:

carbon steel, corrosion, EIS, green inhibitor, green synthesis, Pulicaria odora

Introduction

All types of steel are prone to surface degradation in corrosive environments, particularly acidic media widely used in the petroleum industry for pipelines and other industrial installations, leading to significant material damage. From a thermodynamic standpoint, most metals are inherently unstable in the presence of air and water, with only a few exceptions. However, if the corrosion processes occur slowly and effective protective measures are applied, these materials can perform reliably throughout the intended service life of the system¹. Corrosion is a natural process involving the chemical degradation of materials through reactions with their surrounding environment. Its form and severi-

ty depend on environmental conditions, resulting in either generalized corrosion or localized damage to the material^{2,3}. Various surface modification techniques have been developed to protect metals from corrosion. Chemical treatments using chromates have traditionally been widely used, particularly in the petroleum industry. However, due to the carcinogenic and environmentally dangerous nature of chromates, current research and laws are encouraging safer alternatives. Organic corrosion inhibitors have emerged as a viable option in this context, providing corrosion protection that is both environmentally benign and cost-effective⁴. In particular, green corrosion inhibitors have drawn significant global attention because of their non-toxicity and efficiency in preventing metal deterioration⁵.

At the same time, nanotechnology represents one of the most promising advancements in materials science, providing novel techniques to improve corrosion resistance^{6,7}. Nanotechnology deals with the design, characterization, manufacture, and usage of substances and equipment that have exact control over structure, shape, and size at the nanoscale. Numerous studies have examined green synthesis methodologies for copper oxides, emphasizing its potential for usage in a variety of applications⁸. This involves using a minimum of non-toxic chemical reagents to limit reaction by-products and/or residual ions that could inhibit the intrinsic properties of the final material⁹.

The plant *Pulicaria odora* has been extensively studied by scientists¹⁰. Its multifunctionality, ecological, environmental, socio-economic, industrial, medicinal, pharmaceutical, and cosmetic interests make it increasingly important. This study investigates the use of *Pulicaria odora* leaf extracts as a green corrosion inhibitor¹¹ for SS308 steel in a 1 mol L⁻¹ hydrochloric acid solution. Inhibitory performance was evaluated using stationary (potentiodynamic polarization) and transient (EIS) electrochemical techniques. Additionally, green CuO nanoparticles were developed using the aqueous extract of *Pulicaria odora* leaves and tested for photocatalytic degradation of methylene blue and antimicrobial activity against the bacterial strains.

Materials and methods

Steel preparation and electrolyte

The sample employed in this research was SS308 steel. Its chemical composition is presented in Table 1.

The carbon steel electrode used in the experiments was cut to expose a surface area of 1 cm². To ensure reproducibility, surfaces were mechanically polished using abrasive papers of increasing grit sizes, ranging from 100/250/300/400/600/800/1000 up to the finest grit size of 1200, followed by rinsing with distilled water and drying. The test solution used in this study was hydrochloric acid (HCl) with a concentration of 1 M, prepared by diluting analytical grade 35–37 % HCl with distilled water, resulting in a solution with pH below 1.

Electrochemical methods

Advanced electrochemical techniques, including polarization profiling and electrochemical impedance spectroscopy (EIS), were performed via the state-of-the-art Voltalab PGZ 301 potentiostat/galvanostat system, a multifunctional platform for electrochemical analysis. Tests were implemented in a classic three-electrode configuration housed within a borosilicate glass electrochemical cell,

Table 1 - Chemical composition of SS308 steel

Element	Cu	Fe	Mn	Cr	Co	V	Ni	Mb
Mass (%)	0.13	70.52	1.2	18.45	0.44	0.06	10.01	0.01

comprising a platinum counter electrode and a saturated calomel electrode (SCE) as the reference, ensuring high stability and precision throughout the tests.

Potentials were estimated and reported at the saturated calomel electrode. To reach a quasi-steady state, polarization experiments were performed at a scan rate of 10 mV s⁻¹. The measured potential was between -1200 and 200 mV. Impedance, Z, and phase shift θ , were noted in the 100 kHz to 100 mHz frequency domain. The superimposed AC signal was of 10 mV peak-to-peak amplitude.

Plant preparation

The selected plant species, *Pulicaria odora*, was dried at room temperature in a sheltered, moisture-free setting to maintain its active components. The dried plant was then pulverized with an electric grinder, and kept in sealed containers, away from air, moisture, and light, until required for extraction, (Fig. 1).

Ethanol extract and green copper material preparation

An initial defatting step was performed by immersing 20 g of *Pulicaria odora* biomass into 200 mL of hexane for 15 minutes. Mixture was then filtered using filter paper and a vacuum pump (Fig. 2). The retained plant residue was used for the subsequent CuO nanoparticles synthesis.

For extraction, 160 mL of ethanol was mixed with 40 mL of distilled water. Subsequently, 2 mL of this solution was replaced with 2 mL of acetic acid to optimize the solvent composition. The resulting modified solvent was then used to agitate the plant residue, enhancing the extraction of bioactive compounds.

In addition, CuO nanoparticles were synthesized by adding 500 mL of the ethanolic extract of *Pulicaria odora* to 1000 mL of a copper nitrate solution, which was prepared by dissolving 17 g of Cu(NO₃)₂ in 1 L of distilled water using a magnetic stirrer to ensure complete dissolution of the nitrate. The reactant mixture was maintained at 60 °C for 15 minutes under continuous mechanical stirring. A visible color change from yellow to light brown indicated copper nanoparticles formation (Fig. 3). The mixture was then let to settle, and the yielded pellets were assembled and rinsed many times with distilled water to eliminate impurities, followed by

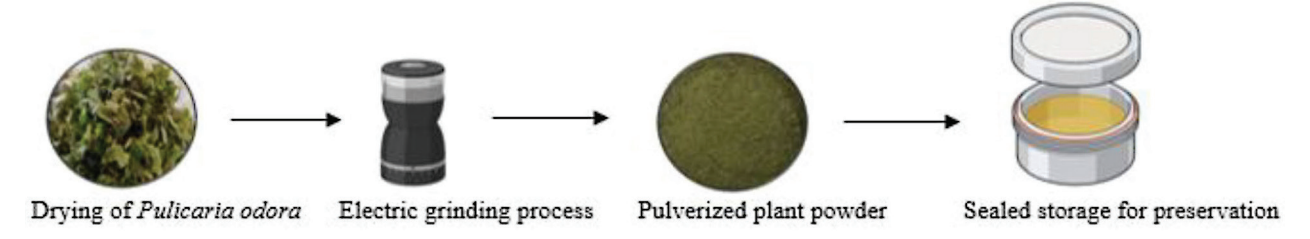


Fig. 1 – Preparation of Pulicaria odora for extraction

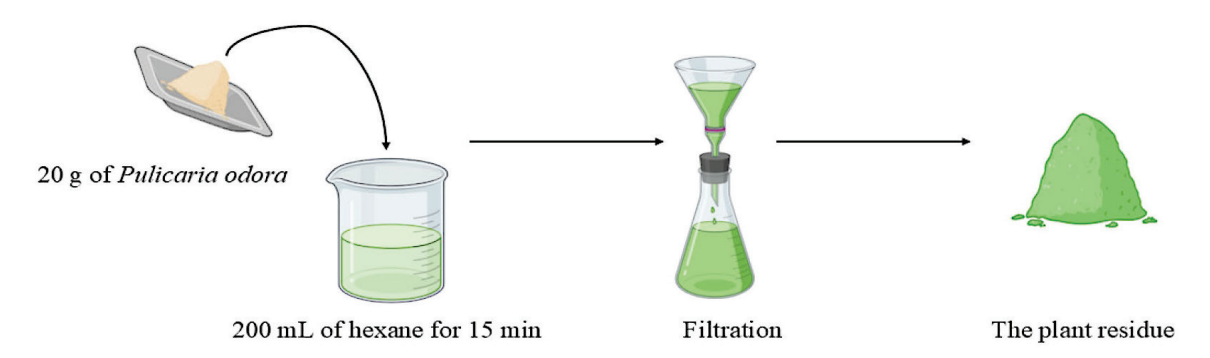
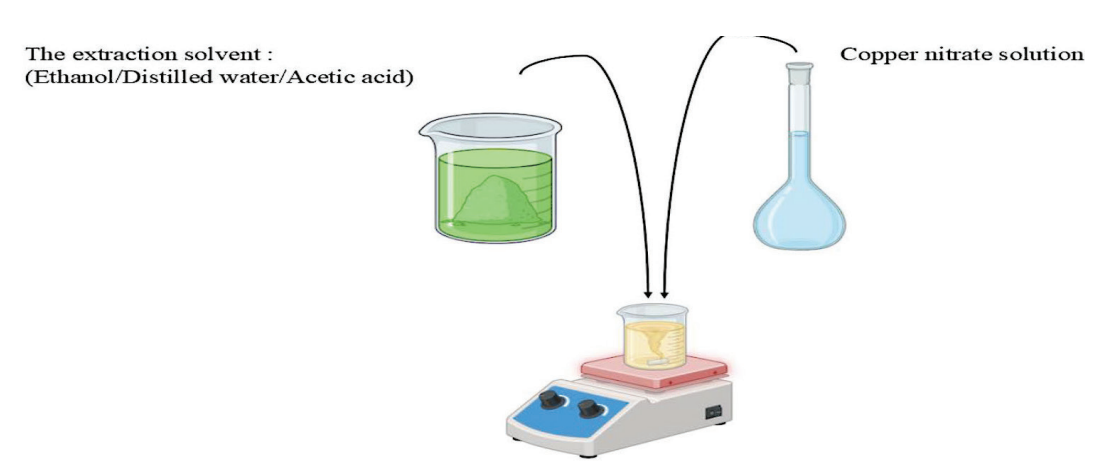


Fig. 2 – Pulicaria odora extract preparation



Maintained at 60 °C for 15 minutes with continuous stirring.

Fig. 3 – Simplified diagram of the mixing process between Cu(NO₃)₂ solution and the bioactive extract of Pulicaria odora

washing with 90 % ethanol. The purified product was dried to obtain CuO nanoparticles in powder form (Fig. 4).

Characterization of synthesized CuO nanoparticles

CuO nanoparticles (CuO NPs) were characterized using X-ray diffraction (XRD) and UV-visible (UV-Vis) spectroscopy. To evaluate the photocatalytic activity of the synthesized silver nanoparticles, we monitored the degradation of Methylene Blue dye. The initial concentration of the Methylene Blue solution was $C_0 = 7.5$ ppm. An amount of 0.2 g of the photocatalyst was added to 200 mL of the

Methylene Blue solution to initiate the degradation process. The variation in the concentration of the irradiated Methylene Blue solution was measured at regular intervals by recording the absorbance of the dye, which absorbs in the visible region, using a UV-Vis spectrophotometer (SHIMADZU 1800) at 664 nm. XRD measurements were performed using Cu-K α radiation to investigate the crystalline structure and phase composition of the nanoparticles. The analysis was conducted using an D8 Advance Eco X-ray diffractometer (Bruker), equipped with a copper tube ($\lambda = 1.54$ Å). This device is designed for the study of polycrystalline samples, whether in powder form or as bulk materials. It operates in

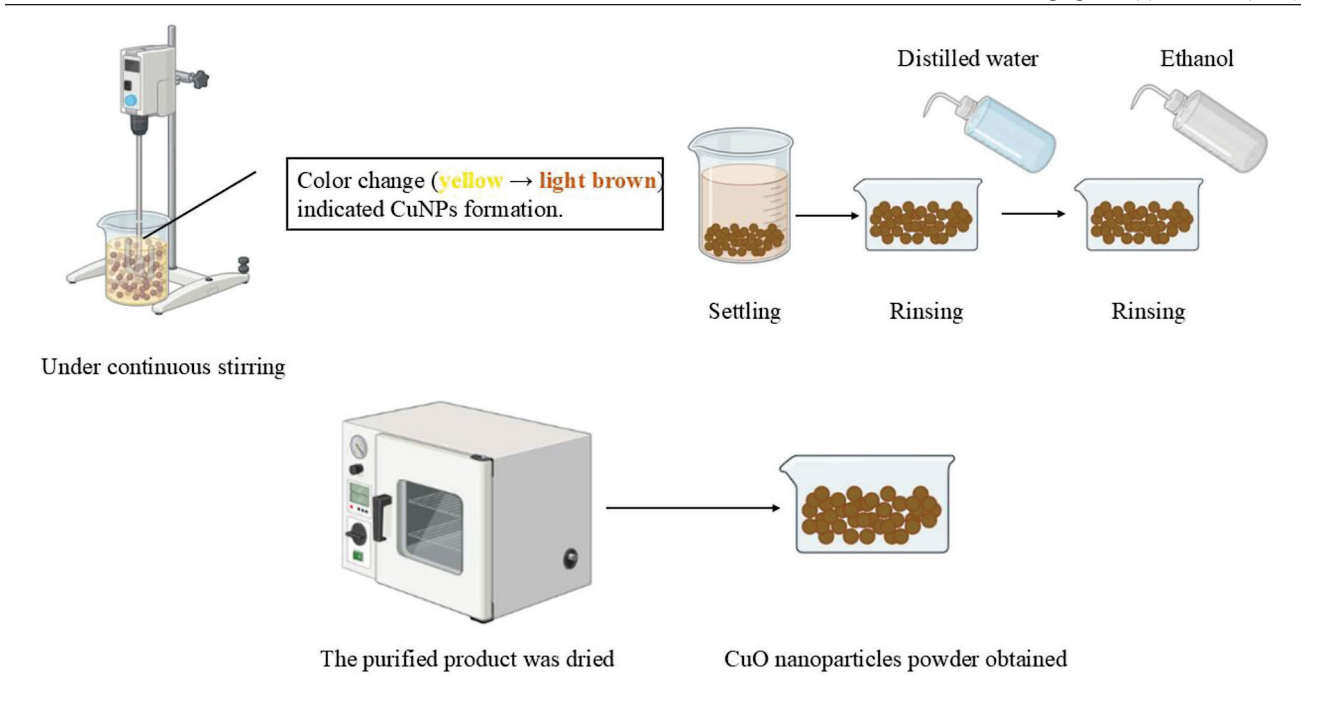


Fig. 4 - Process for synthesizing CuO nanoparticles using Pulicaria odora

Bragg-Brentano geometry under "Theta-Theta" mode, where the sample remains horizontal throughout the measurement, with a focusing radius of 500 mm.

Antimicrobial activity

A study was conducted to evaluate the antimicrobial efficiency of CuO NPs synthesized from Pulicaria odora against various bacterial strains from the American Type Culture Collection (ATCC). The strains tested comprised Staphylococcus aureus ATCC® 6538, a Gram-positive bacterium, as well as Escherichia coli ATCC® 25922 and Pseudomonas aeruginosa ATCC® 27853, Gram-negative bacteria. All the bacterial strains used in this study were supplied by the Institut Pasteur d'Algérie. An agar diffusion test was conducted to determine whether copper oxide nanoparticles synthesized from Pulicaria odora inhibited bacterial growth. Every bacterial strain was cultured in nutrient broth for 18 hours at 37 °C. The inoculum of bacterial isolates was generated aseptically, and the cell density was set to 106 CFU mL⁻¹ or 0.55 McFarland standard to enable consistent reseeding of Agar Muller Hinton plates with a sterile swab. Green copper oxide nanoparticles were successively diluted from 2048 $\mu g \text{ mL}^{-1}$ to 1024, 512, 256, 128, 64, and 32 $\mu g \text{ mL}^{-1}$. Disks were positioned at specific locations on the gel-filled medium and filled with various amounts of nanoparticle solution (30 µL for each). After 24 hours of incubation at 37 °C, Petri dishes were gathered, and the inhibition areas that developed within the disks were examined and measured.

Results and discussion

Inhibition of carbon steel corrosion with Pulicaria odora leaf extract

Polarization curves

In the log I = f(E) representations, (Fig. 5), two distinct segments can be observed for each curve. A cathodic segment corresponds to an oxygen reduction reaction at the steel surface, and an anodic segment represents an oxidation reaction¹².

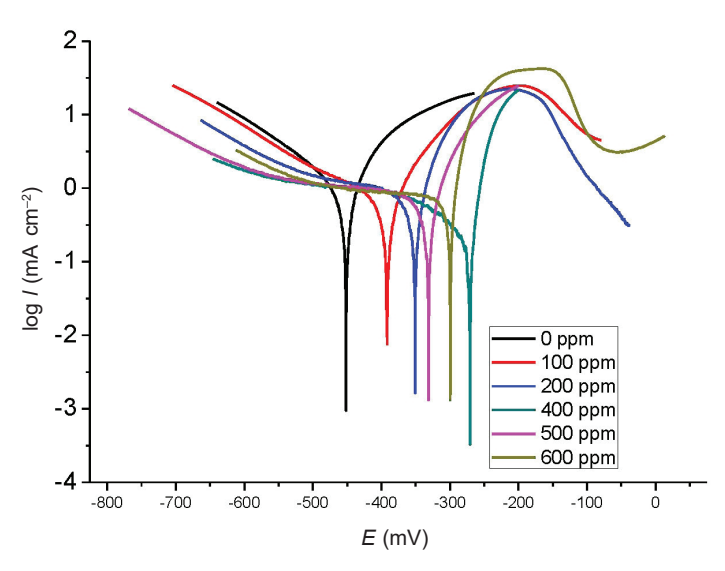


Fig. 5 – Polarization curves of SS308 in 1 mol L⁻¹ HCl, with and without incorporation of multiple amounts of Pulicaria odora extract at 25 °C

Table 2 – Electrochemical parameters and corresponding inhibition efficiency of carbon steel at various concentrations of Pulicaria odora

C (ppm)	$E_{\rm corr} \ ({ m mV})$	I _{corr} (mA cm ⁻²)	$B_{\rm a}$ (mV dec ⁻¹)	$\frac{B_{\rm c}}{({\rm mV~dec^{-1}})}$	E (%)
Blank	-450.0	1.043	126.2	-157.5	/
100	-390.0	0.412	88.1	-168.7	60.50
200	-350.5	0.162	54.5	-183.1	84.40
400	-270.8	0.136	17.0	-297.8	86.90
500	-331.0	0.054	48.0	-185.9	95.00
600	-299.4	0.189	72.3	-257.9	81.86

Corrosion current density (I_{corr}) , corrosion potential (E_{corr}) , cathodic and anodic Tafel slopes (B_{c}) and B_{a} , inhibition effectiveness (E/%), and surface coverage (θ) values for various extract doses are presented in Table 2. Inhibitor effectiveness (E/%) and surface coverage (θ) were calculated using the following equations:

$$\theta = \frac{I_{\text{corr}} - I_{\text{corr(inh)}}}{I_{\text{corr}}} \tag{1}$$

$$E/\% = \theta \cdot 100 \tag{2}$$

where, θ is the inhibitor surface coverage on the metal surface, I_{corr} is the corrosion current density value without inhibitor, and $I_{\text{corr}(\text{inh})}$ is the corrosion current density value with inhibitor.

Results in Table 2 show that corrosion current densities (I_{corr}) decreases with increasing extract concentration, while the inhibitory efficiency E/% increases with rising inhibitor doses, reaching an upper limit of 95 % at 500 ppm. Beyond 500 ppm, inhibition efficiency decreases significantly. Inhibi-

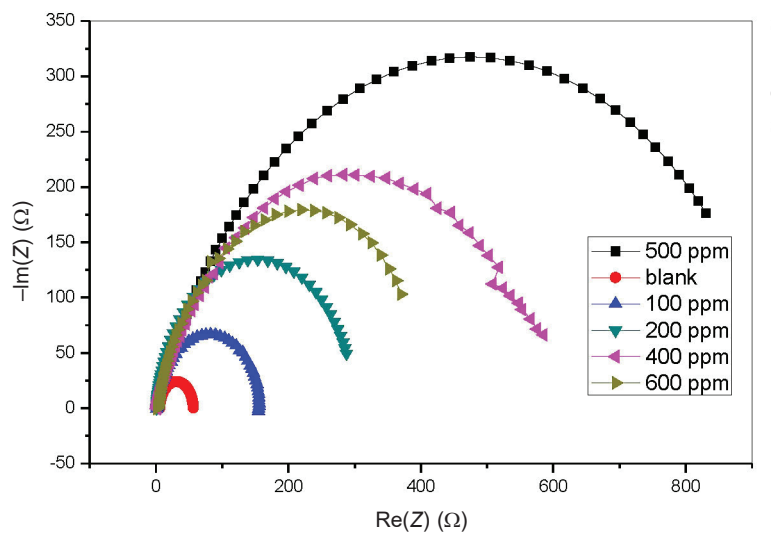


Fig. 6 – Nyquist plots of Pulicaria odora extracts at varying concentrations at 25 °C

tor injection into the acidic solution alters the Tafel slope values, indicating that both anodic and cathodic processes were impacted. The corrosion potential shifts to more positive values in the presence of the inhibitor. According to Ferreira *et al.*¹³ and Li *et al.*¹⁴, a potential shift greater than 85 mV compared to the blank classifies the inhibitor as anodic or cathodic¹⁵. In this study, the extract largely acted as an anodic inhibitor, as shown by a shift of more than 85 mV¹⁵. The corrosion potentials of the electrode in the presence of the inhibitor tended to shift toward more anodic values compared to the potential of the electrode without the inhibitor¹⁶.

Electrochemical impedance spectroscopy (EIS)

EIS provides insights into corrosion and adsorption phenomena^{17,18}.

Nyquist plots obtained from EIS measurements for steel immersed in 1 mol L⁻¹ HCl with and without *Pulicaria odora* extract are shown in Fig. 6. Increasing the concentration of *Pulicaria odora* extracts increased impedance of the steel.

Moreover, a single capacitive loop was observed at high frequency, indicating the presence of a one-time constant. The semicircles in the Nyquist plots for solid electrodes are slightly distorted. Solid electrodes typically exhibit deviations from ideal behavior. This dispersion was attributed to surface roughness and other inhomogeneities of the solid electrode¹⁹. The abnormal dispersion of capacitance can be modeled by an element known as a Constant Phase Element (CPE)²⁰. The use of CPE to account for non-ideal conditions on solid surfaces has been previously described¹⁹.

Furthermore, the addition of *Pulicaria odora* extract leads to an increase in the diameter of the semicircles compared to the blank solution, indicating the adsorption of inhibitor molecules onto the steel surface and the formation of an organic film.

The EIS results were well fitted using the equivalent electrical circuit shown in Fig. 7. This simulated circuit consisted of an electrolyte resis-

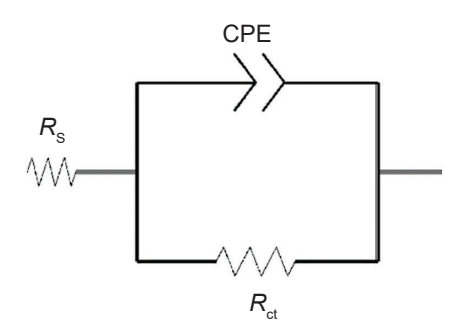


Fig. 7 – Equivalent circuit modeling of steel

tance (R_s) in series with a constant phase element (CPE) in parallel with a charge transfer resistance (R_{ct}) . The impedance of a CPE can be defined by the following equation:

$$Z_{\text{CPE}} = Q^{-2} \left(j\omega \right)^{-n} (3) \tag{3}$$

where Q is the CPE constant; j is the imaginary unit $(-1)^{1/2}$; n is the CPE exponent, which can be used as an indicator of surface heterogeneity or roughness; ω is the angular frequency at which the imaginary component of the impedance is maximal:

$$\omega = 2\pi f \tag{4}$$

The relationship between the double-layer capacitance $C_{\rm dl}$ and Q is given by the following equation:

$$C_{\rm dl} = \left(QR_{\rm ct}^{1-n}\right)^{1/n} \tag{5}$$

The inhibitory effectiveness of steel corrosion is determined by the charge transfer resistance $(R_{\rm ct})$ readings employing the formula below:

$$E/\% = \frac{R_{\rm ct} - R_{\rm ct}^0}{R_{\rm ct}} \cdot 100 \tag{6}$$

where R_{ct}^0 and R_{ct} are charge transfer resistances in the absence and presence of the inhibitor, respectively²⁷.

The impedance parameters obtained by fitting the EIS data using the equivalent circuit are summarized in Table 3.

The inhibition efficiency of *Pulicaria odora* extracts, calculated from these parameters, follows the same trend as the charge transfer resistance, and reaches a maximum value of 94.6 % at a concentration of 500 ppm of *Pulicaria odora* extract²¹.

The charge transfer resistance ($R_{\rm cl}$) value established without the inhibitor reveals steel degradation within the first hours of soaking, which is usually due to a conductive layer of corrosive substances^{22,23}. As the extract quantity rises, charge transfer resistance ($R_{\rm cl}$) increases and the double-layer capacitance ($C_{\rm dl}$) decreases until the extract

Table 3 – Electrochemical impedance values of carbon steel in 1 mol L⁻¹ hydrochloric acid solution containing different concentrations of Pulicaria odora

C (ppm)	$R_{\rm s}(\Omega~{\rm cm}^2)$	CPE _{dl} (F cm ⁻²)	n	$R_{\rm ct} (\Omega {\rm cm}^2)$	E (%)
Blank	5.66	$0.22 \cdot 10^{-3}$	0.97	50.79	/
100	1.47	$0.74 \cdot 10^{-3}$	0.88	161	68.4
200	1.21	$0.90 \cdot 10^{-3}$	0.93	301	83.1
400	0.98	$0.26 \cdot 10^{-3}$	0.79	598.8	91.5
500	1.73	$0.37 \cdot 10^{-3}$	0.75	950	94.6
600	1.64	0.46 · 10-3	0.84	485	89.5

concentration reaches 500 ppm. This occurs due to the forming of a protective coating on the metal surface. The drop in Q can be associated with a reduction in the dielectric constant and/or a rise in the double-layer thickness²⁴. In simple terms, the addition of inhibitor limits the double-layer thickness, adjusts the oxide layer structure, and consequently lowers the Q value^{25,26}.

On the impedance curve, a rise in the dimension of the loops indicates that film characteristics have improved.

Adsorption isotherms

Organic chemicals limit metal corrosion by adsorption on the metal surface. Adsorption isotherms are thus a significant supplement that may aid in determining how these organic molecules adsorb on the surface. To derive the isotherm, one has to estimate the surface coverage as a function of the inhibitor amount.

Various isotherms were examined to determine the adsorption type appropriate for the system investigated. The isotherms show that the surface coverage (θ) can be related to the inhibitor concentration $C_{\rm inh}$ using the well-known Langmuir equation:

$$\frac{C_{\rm inh}}{\theta} = \frac{1}{K_{\rm ads}} + C_{\rm inh} \tag{7}$$

where $C_{\rm inh}$ is the concentration of the inhibitor (ppm), $K_{\rm ads}$ is the adsorption equilibrium constant, θ is the surface coverage, and 1000 corresponds to the concentration of water molecules expressed in g L⁻¹. R is the universal gas constant, and T is the absolute temperature.

Fig. 8 illustrates the linear relationship between C_{inh}/θ and C_{inh} at 298 K for the *Pulicaria odora* extract inhibitor. The linearity of this relationship, with a regression coefficient (R^2) of 0.99, indicates good conformity with the Langmuir adsorption isotherm. The slope and intercept of the linear plot were determined, with the slope recorded as -0.92, i.e., close to unity. This slight deviation from ideal behavior may be attributed to interactions among the adsorbed species on the metal surface, such as mutual repulsion or attraction²⁷. These findings support the adsorption of inhibitor molecules onto the steel surface, in line with the assumptions of the Langmuir isotherm, which posits monolayer adsorption with no lateral interaction between adsorbed species.

The adsorption free energy ($\Delta G_{\rm ads}^{\circ}$) could be obtained by equation (8)^{5,6}

$$\Delta G_{\text{ads}}^{\circ} = -RT \ln \left(1000 K_{\text{ads}} \right) \tag{8}$$

where R and T represent the molar gas constant (8.314 J mol⁻¹ K⁻¹) and absolute temperature (298

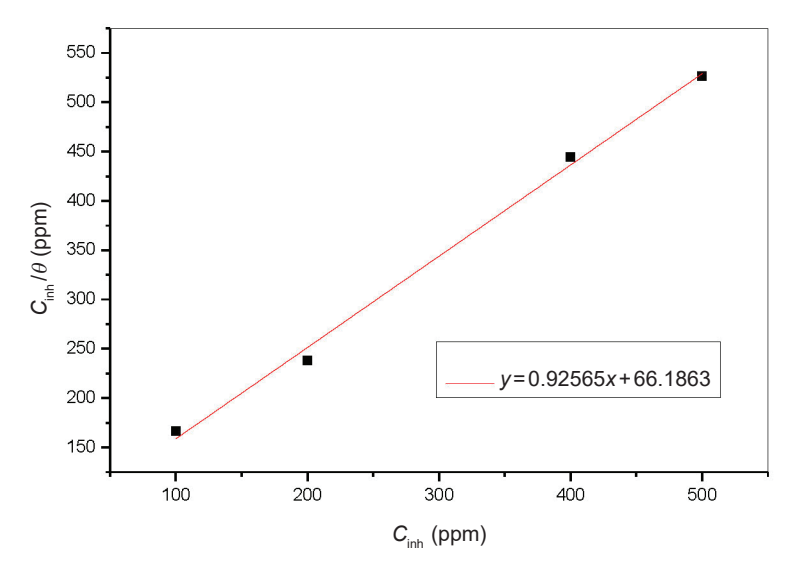


Fig. 8 – Langmuir adsorption isotherm of steel with varying doses of Pulicaria odora leaf extracts at 25 °C

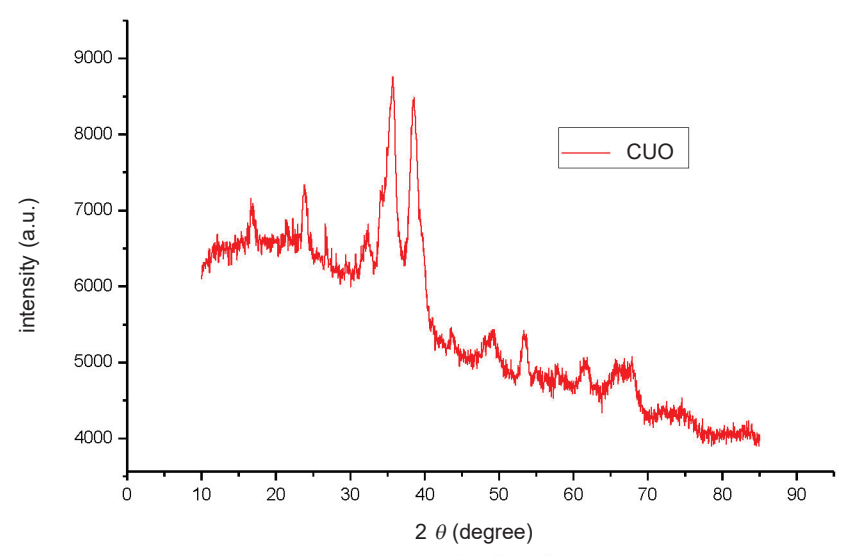


Fig. 9 – XRD results of plant-based copper oxide nanoparticles

K), respectively. By calculation, the $K_{\rm ads}$ value was about $-23.84~{\rm kJ~mol^{-1}}$. The negative value of $\Delta G^{\circ}_{\rm ads}$ confirms the spontaneous nature of the adsorption process and the thermodynamic stability of the adsorbed layer on the metallic surface. This magnitude also suggests that the adsorption mechanism was predominantly physical in nature.

According to literature, $\Delta G_{\rm ads}^{\circ}$ values more negative than $-40~{\rm kJ~mol^{-1}}$ typically indicate chemisorption, whereas values between $-20~{\rm and}~-40~{\rm kJ~mol^{-1}}$ are indicative of electrostatic interactions and/or physisorption⁶. In this study, the obtained $\Delta G_{\rm ads}^{\circ}$ values fall within the $-20~{\rm to}~-40~{\rm kJ~mol^{-1}}$ range, confirming that both physical interactions contribute to the adsorption mechanism of the *Pulicaria odora* inhibitor on the carbon steel surface.

XRD analysis

Plant-derived CuO nanoparticles phase composition was assessed using X-ray diffraction (XRD) as highlighted in Fig. 9, revealing 12 distinct diffraction peaks. Bragg diffraction peaks observed at 2θ values of 32.14°, 35.82°, 38.48°, 49.11°, 53.40°, 58.1°, 61.59°, 66.89°, 72.1°, and 74.66°, were attributed to the (110), (–111), (111), (–202), (020), (202), (–113), (–311), (311), and (–222) crystallographic planes, respectively. The XRD pattern confirmed that the CuO nanoparticles, synthesized from the plant extract, exhibited a face-centered cubic (FCC) crystalline structure, as per the Joint Committee on Powder Diffraction Standards (JCPDS) file number 80–1268. The prominent

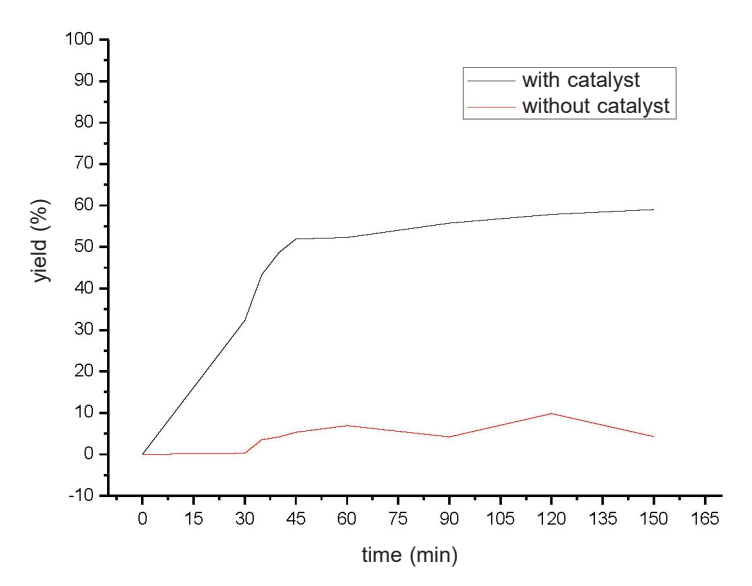


Fig. 10 – Degradation efficiency of Methylene Blue with/without copper oxide nanoparticles catalyst

peaks in the 2θ range of $35{\text -}39^\circ$ further corroborate CuO nanoparticles formation, in line with previous studies^{29,30}.

Photocatalytic activity

In this section, we evaluated the photocatalytic activity of CuO nanoparticles (NPs) for the degradation of Methylene Blue (a model dye compound), both in the presence and absence of the catalyst. The first step of the experiment was dedicated to the adsorption of the dye from the solution onto the surface of the catalyst. This adsorption phenomenon leads to a more or less significant decrease in the dye concentration in solution, depending on the catalyst/dye system.

To accurately study the photocatalytic degradation kinetics, irradiation must begin only after the adsorption equilibrium has been reached. The adsorption step is carried out in the dark until the equilibrium concentration is achieved. In practice, after approximately 30 minutes, equilibrium was established, with only minimal degradation observed. However, upon exposure to light using a lamp, the degradation efficiency increased significantly.

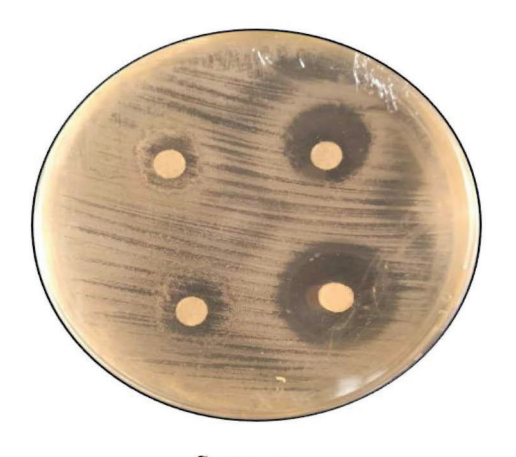
In photocatalytic reduction of Methylene Blue, 250 mL of a 15 ppm Methylene Blue solution was put in a quartz container. An amount of 0.2 g of CuO nanoparticles catalyst was added to the mixture, which was then subjected to UV-C lamps. Methylene Blue amount was measured over time using UV spectroscopy at a wavelength of 664 nm. The measured concentration variations were then used to calculate the effectiveness of photocatalytic reduction as indicated by decolorization:

Effectiveness (%) =
$$\frac{C_0 - C}{C_0} \cdot 100$$
 (9)

As shown in Fig. 10, the decolorization effectiveness increased over time. A control experiment without the catalyst showed no visible color change even after three days, confirming the catalyst's essential role. In contrast, the presence of CuO NPs led to an 80 % decolorization within just 150 minutes. The catalyst facilitates electron transfer between Methylene Blue molecules, which adsorb onto its surface and gradually lose their color³¹. These findings demonstrate the high effectiveness of CuO NPs in promoting Methylene Blue degradation³².

Antimicrobial activity

The study of the antimicrobial properties of CuO nanoparticles (NPs) synthesized from *Pulicaria odora* extract produced promising results. The inhibition diameters measured at different concentrations of nanoparticles revealed significant inhibi-





P. aeruginosa

Fig. 11 – Illustration of CuO nanoparticles antimicrobial activity essay

Table 4 – CuO NPs antimicrobial activity

	Inhibition diameter (mm)							
Concentration	2048 μg mL ⁻¹	1024 μg mL ⁻¹	512 μg mL ⁻¹	256 μg mL ⁻¹	128 μg mL ⁻¹	64 μg mL ⁻¹	$\begin{array}{c} 32 \\ \mu g \ mL^{-1} \end{array}$	15 μg mL ⁻¹
Escherichia coli	20.25 ±1.33	19.75±1.33	18.50±0.71	17.75±1.14	12.66±0.89	9.25±0.66	9±0.35	Nd
Staphylococcus aureus	20.66 ± 1.71	18.75 ± 1.33	13.75 ± 0.47	11.50 ± 0.89	9.75 ± 0.47	9.00 ± 0.33	Nd	Nd
Pseudomonas aeruginosa	28.15 ± 1.89	26.15±1.71	24.50±0.89	20.25±1.33	15.75±0.33	11.33 ± 0.71	10 ± 0.47	Nd

tory activity versus the bacterial strains assessed, namely *E. coli*, *S. aureus*, and *P. aeruginosa*. A dose-dependent trend was observed (Fig. 11), where a boost in NP concentration correlated with larger inhibition diameters, suggesting a direct relationship between NP concentration and their antimicrobial activity.

However, variations in the sensitivity of bacterial strains were also noted, indicating that the response to CuO nanoparticles may be influenced by specific bacterial characteristics. For example, P. aeruginosa (28.15±1.89 mm) showed relatively higher sensitivity than S. aureus (20.66 \pm 1.71 mm) to lower concentrations of nanoparticles, Table 4, while S. aureus appeared to be more sensitive to higher concentrations than E. coli. These findings are similar to those of previous studies on the antibacterial activity of Pulicaria odora plant33-35. Furthermore, in some cases, the antimicrobial activity of NPs was below the detection limit at certain concentrations, highlighting the need to consider higher concentrations or other detection methods for further analysis. These results highlight the promising potential of CuO nanoparticles synthesized from Pulicaria odora extract as effective antimicrobial agents. They also highlight the crucial importance of better understanding the specific sensitivity of different bacterial strains. This detailed understanding is essential to optimize the use of these nanoparticles in various medical and environmental applications, where their efficacy could have a significant impact.

Conclusion

This study demonstrates that *Pulicaria odora* leaf extract is an effective green inhibitor for the corrosion of steel in corrosive environments. Electrochemical analyses confirmed that the extract primarily acts as an anodic-type inhibitor, achieving a maximum inhibition efficiency of approximately 95% at a concentration of 500 ppm—an observation generally consistent with both polarization and electrochemical impedance spectroscopy (EIS) methods. The inhibitor adsorption onto the steel surface follows the Langmuir isotherm, with nega-

tive $\Delta G_{\rm ads}^{\circ}$ values revealing a spontaneous and predominantly physical adsorption process. Additionally, *Pulicaria odora* extract was successfully applied to synthesize CuO nanoparticles, showing promising photocatalytic activity in Methylene Blue degradation. These findings highlight the dual functionality of *Pulicaria odora* as both a corrosion inhibitor and a sustainable source for nanomaterial synthesis, offering significant potential for eco-friendly industrial applications.

References

- Short, A., Introduction to corrosion and its control: Corrosion in metals and its prevention, National Corrosion Service, NPL (2003) 1.
- Zeghloul, A., Mécanismes d'endommagement des structures métalliques, (2000) 5.
 www.mim.univ-metz.fr/formations/documents/1/cours DM-Luno.pdf
- Nimmo, B., Hinds, G., Beginners guide to corrosion, National Physical Laboratory (NPL) (2003) 1.
- Bommersbach, P., Évolution des propriétés d'un film inhibiteur de corrosion sous influence de la température et de conditions hydrodynamiques, caractérisation par techniques électrochimiques, Ph.D. Thesis, INSA de Lyon, Génie des matériaux (2005) 154.
- Khelfaoui, M., Zouied, D., Bouzenad, N., Abdennouri, A., Boussouf, I., Damous, M., Belhocine, Y., Antimicrobial activity and high anticorrosion efficiency of Carpobrotus acinaciformis L. extracts against C1020 carbon steel corrosion in a hydrochloric acid medium, Chem. Biochem. Eng. Q. 39 (2025) 15. doi: https://doi.org/10.15255/CABEQ.2024.2397
- Zouied, D., Chettah, W., Khelfaoui, M., Bouzenad, N., Abdennouri, A., Dob, K., Zouaoui, E., The use of Arum italicum root extracts for protection against corrosion and green synthesis of silver nanoparticles: Investigation of their photocatalytic and antimicrobial properties, Glob.

Nest J. **27** (2024) 206931. doi: https://doi.org/10.30955/gnj.06931

- 7. Khan, F., Shariq, M., Asif, M., Siddiqui, M. A., Malan, P., Ahmad, F., Green nanotechnology: Plant-mediated nanoparticle synthesis and application, Nanomaterials 12 (2022) 673. doi: https://doi.org/10.3390/nano12040673
- 8. *Salem*, *S.*, A mini review on green nanotechnology and its development in biological effects, Arch. Microbiol. **205** (2023) 128. doi: https://doi.org/10.1007/s00203-023-03467-2
- 9. *Bordiwala, R. V.*, Green synthesis and applications of metal nanoparticles a review article, Results Chem. **5** (2023) 100832.

doi: https://doi.org/10.1016/j.rechem.2023.100832

- Saidani, K., Touati, N., Merzouk, H., Boussaa, H., Bedjou, F., Oomah, B. D., Phenolic compounds and antioxidant and antimicrobial activities of *Pulicaria odora* extract, Curr. Bioact. Compd. 19 (2023) 11. doi: https://doi.org/10.2174/1573407218666220404094002
- Ezoubeiri, A., Gadhi, C. A., Fdil, N., Benharref, A., Jana, M., Vanhaelen, M., Isolation and antimicrobial activity of two phenolic compounds from *Pulicaria odora*, J. Ethnopharmacol. 99 (2005) 287. doi: https://doi.org/10.1016/j.jep.2005.02.015
- 12. Dob, K., Zouaoui, E., Zouied, D., Corrosion inhibition of Curcuma and Saffron on A106 Gr B carbon steel in 3 % NaCl medium, Anti-Corros. Methods Mater. 65 (2018) 225. doi: https://doi.org/10.1108/ACMM-06-2017-1805
- Ferreira, E. S., Giacomelli, C., Giacomelli, F. C., Spinelli, A., Evaluation of the inhibitor effect of L-ascorbic acid on the corrosion of mild steel, Mater. Chem. Phys. 83 (2004) 129.
 - doi: https://doi.org/10.1016/j.matchemphys.2003.09.020
- 14. *Li, W. H., He, Q., Zhang, S. T., Pei, C. L., Hou, B. R.*, Some new triazole derivatives as inhibitors for mild steel corrosion in acidic medium, J. Appl. Electrochem. **38** (2008) 289. doi: https://doi.org/10.1007/s10800-007-9437-7
- Dob, K., Zouaoui, E., Ammouchi, N., Zouied, D., Corrosion inhibition of A106 Gr B carbon steel by *Thapsia garganica* extracts in 1 M hydrochloric acid, Anal. Bioanal. Electrochem. 11 (2019) 1500.
- Zouied, D., Zouaoui, E., Medjram, M. S., Chikha, O., Dob, K., The para hydroxy acetanilide and acetanilide mixture for the protection from corrosion of alloyed zinc, ACMM 65 (1) (2018) 1.
 doi: https://doi.org/10.1108/ACMM-02-2017-1754
- Macdonald, J. R., Impedance Spectroscopy, 3rd ed., John Wiley & Sons, New York, 1987. doi: https://doi.org/10.1007/BF02368532
- Aït Aghzzaf, A., Rhouta, B., Rocca, E., Khalil, A., Steinmetz, J., Corrosion inhibition of zinc by calcium-exchanged beidellite clay mineral: A new smart corrosion inhibitor, Corros. Sci. 80 (2013) 46. doi: https://doi.org/10.1016/j.corsci.2013.10.037
- Sharma, S., Ganjoo, R., Kr. Saha, S., Kang, N., Thakur, A., Assad, H., Sharma, V., Kumar, A., Experimental and theoretical analysis of baclofen as a potential corrosion inhibitor for mild steel surface in HCl medium, J. Adhes. Sci. Technol. 36 (19) (2022) 2067. doi: https://doi.org/10.1080/01694243.2021.2000230
- Bentrah, H., Rahali, Y., Chala, A., Gum Arabic as an ecofriendly inhibitor for API 5L X42 pipeline steel in HCl medium, Corros. Sci. 82 (2014) 426. doi: https://doi.org/10.1016/j.corsci.2013.12.018
- El-Taib Heakal, F., Fouda, A. S., Radwan, M. S., Some new thiadiazole derivatives as cor rosion inhibitors for 1018 carbon steel dissolution in sodium chloride solution, Int. J. Electrochem. Sci. 6 (8) (2011) 3140. doi: https://doi.org/10.1016/S1452-3981(23)18242-3
- 22. Zhao, T., Mu, G., The adsorption and corrosion inhibition of anionic surfactants on alumin ium surface in hydrochloric acid, Corros. Sci. 41 (1999) 1937. doi: https://doi.org/10.1016/S0010-938X(99)00029-3

- Zouied, D., Zouaoui, E., Medjram, M. S., Chikha, O., Dob, K., The para-hydroxyacetanilide and acetanilide mixture for the protection from corrosion of alloyed zinc, Anti-Corros. Methods Mater. 65 (2018) 1. doi: https://doi.org/10.1108/ACMM-02-2017-1754
- 24. Zhang, B., He, C., Chen, X., Tian, Z., Li, F., The synergistic effect of polyamidoamine den drimers and sodium silicate on the corrosion of carbon steel in soft water, Corros. Sci. 90 (2015) 585.
 - doi: https://doi.org/10.1016/j.corsci.2014.10.054
- Al-Sabagh, A. M., Migahed, M. A., Awad, H. S., Reactivity of polyester aliphatic amine surfactants as corrosion inhibitors for carbon steel in formation water (deep well water), Corros. Sci. 48 (2006) 813. doi: https://doi.org/10.1016/j.corsci.2005.04.009
- Deng, S., Li, X., Fu, H., Two pyrazine derivatives as inhibitors of the cold rolled steel cor rosion in hydrochloric acid solution, Corros. Sci. 53 (2011) 822. doi: https://doi.org/10.1016/j.corsci.2010.11.019
- Safak, S., Duran, B., Yurt, A., Türkoğlu, G., Schiff bases as corrosion inhibitors for aluminium in HCl solution, Corros. Sci. 54 (2012) 251.
 doi: https://doi.org/10.1016/j.corsci.2011.09.026
- Yuce, A., Kardas, G., Adsorption and inhibition effect of 2-thiohydantoin on mild steel corrosion in 0.1 M HCl, Corros. Sci. 58 (2012) 86. doi: https://doi.org/10.1016/j.corsci.2012.01.013
- 29. Eid, A. M., Fouda, A., Hassan, S. E. D., Hamza, M. F., Alharbi, N. K., Elkelish, A., Alharthi, A., Salem, W. M., Plant-based copper oxide nanoparticles: Biosynthesis, characterization, antibacterial activity, tanning wastewater treatment, and heavy metals sorption, Catalysts 13 (2023) 348. doi: https://doi.org/10.3390/catal13020348
- 30. *Naz, S., Gul, A., Zia, M.*, Toxicity of copper oxide nanoparticles: A review study, IET Nanobiotechnol. **14** (2020) 1. doi: https://doi.org/10.1049/iet-nbt.2019.0176
- 31. *He, C., Liu, Z., Lu, Y., Huang, L., Yang, Y.,* Graphene-supported silver nanoparticles with high activities toward chemical catalytic reduction of methylene blue and electrocatalytic oxidation of hydrazine, Int. J. Electrochem. Sci. **11** (2016) 9566. doi: https://doi.org/10.20964/2016.11.72
- 32. Ekinci, A., Kutluay, S., Şahin, Ö., Baytar, O., Antibacterial activity of *Pulicaria odora* species from Turkey, Int. J. Phytoremediation **25** (2022) 789. doi: https://doi.org/10.1080/15226514.2022.2109588
- Saidani, K., Touati, N., Hassaini, Y., Kasri, A., Bedjou, F., Antibacterial activity of *Pulicaria odora* leaf phenolics collected in Algeria, Anti-Infect. Agents 21 (2023) 54. doi: https://doi.org/10.2174/2211352520666220501163744
- 34. Hammiche, H., Saidani, K., Ouazene, N., Touati, N., Boudries, H., Bedjou, F., Antibacterial activity of phenolic compounds of *Pulicaria odora*, wild plant in northern Algeria, Int. Food Res. J. 25 (5) (2018) 2121.
- 35. Nath, E. Ö., Bilgin, M., Gurdal, B., Antimicrobial activity of *Pulicaria* species from Turkey, Experimed. **11** (2021) 195.
 - doi: https://doi.org/10.26650/experimed.2021.986570